



Modeling and simulation of a three-dimensional tumor spheroid

Catharina Meyer

March 30, 2015

Supervisors: *Dirke Imig*
Wolfgang Halter
Examiners: *Prof. Dr-Ing. Allgöwer*
Prof. Dr. Radde

University of Stuttgart
Institute for Systems Theory and Automatic Control
Prof. Dr.-Ing. Frank Allgöwer

Eidesstattliche Erklärung

Ich versichere hiermit, dass ich, Catharina Meyer, die vorliegende Arbeit selbstständig angefertigt, keine anderen als die angegebenen Hilfsmittel benutzt und sowohl wörtliche, als auch sinngemäß entlehnte Stellen als solche kenntlich gemacht habe. Die Arbeit hat in gleicher oder ähnlicher Form noch keiner anderen Prüfungsbehörde vorgelegen und wurde nicht veröffentlicht. Das elektronische Exemplar stimmt mit den anderen überein.

Ort, Datum

Unterschrift

Mitwirkung

Die Arbeit basiert auf dem mathematischen Modell und dem Simulationsalgorithmus publiziert in Imig *et al.* (2015). Die Aufgabenstellung von der Betreuerin Dirke Imig war das bestehende Modell um eine dritte Dimension zu erweitern, so dass Medikamentendiffusion und Änderung der Wachstumsrate im Sphäroid enthalten sind. Die Vorgehensweise und Methoden um dieses Ziel zu erreichen wurden selbstständig von Catharina Meyer erarbeitet und implementiert.

Contents

List of Figures	III
Nomenclature	V
1 Introduction	1
I Propaedeuticum	3
2 Biological Background	5
2.1 Tumor Formation	5
2.2 Pathway of Apoptosis	6
2.3 The Potential Therapeutic TRAIL	8
3 Three-dimensional Models of Tumor Spheroids	11
3.1 Experimental Models	11
3.2 <i>In Silico</i> Modeling Approaches	13
II Bachelor thesis: Modeling and simulation of a three-dimensional tumor spheroid	15
4 Original Model	17
4.1 Intracellular ODE Model	17
4.2 Simulation Algorithm	20
5 Three-dimensional Model	21
5.1 Biological System	21
5.2 Model of Extracellular Substrate Dynamics	22
5.2.1 Extracellular TRAIL Dynamics	23
5.2.2 Extracellular Glucose Dynamics	25
5.3 Model of Intracellular Substrate Dynamics	27

5.3.1	Intracellular TRAIL Dynamics	27
5.3.2	Intracellular Glucose Dynamics	29
6	Implementation of Simulation Algorithm	31
6.1	Numerical Solution	31
6.2	Modifications	32
6.3	Structure	33
7	Parameter and Validation	37
7.1	Concentration of Glucose, Uptake Rate and Growth Rate . . .	37
7.2	TRAIL Concentration	41
8	Analysis and Simulation	45
8.1	Analysis of Computational Effort	45
8.2	Simulation	46
9	Summary, Conclusions and Outlook	51
	Bibliography	52

List of Figures

2.1	Schematic cross section of an avascular tumor in comparison to a central section of an <i>in vitro</i> spheroid	6
2.2	Activation of the cell-extrinsic and cell-intrinsic apoptosis pathways by Apo2L/TRAIL	7
2.3	TRAIL receptors and their function	9
3.1	Characteristics of MCTS in comparison to avascular microtumors, micrometastases and intercapillary tumor microregions	12
4.1	Original reaction network	17
4.2	Scheme for the original simulation algorithm	19
5.1	Extracellular reaction network	23
5.2	Extended reaction network	28
6.1	Scheme for the extended simulation algorithm	34
7.1	Steady state distribution of glucose concentration in a spheroid	39
7.2	Steady state rates of glucose uptake and cell growth in a spheroid	40
7.3	Concentration of TRAIL after 24h and 96h diffusion	42
7.4	Monolayer under TRAIL treatment	43
8.1	Comparison of Simulation in 2D and 3D	47
8.2	TRAIL concentration in the spheroid after 72h simulation . . .	48

Nomenclature

C	Concentration
c	Extracellular concentration
$C3$	Procaspase 3
$C3^*$	Activated caspase 3
$C3^* : IAP$	Complex of $C3^*$ and IAP
$C8$	Procaspase 8
$C8^*$	Activated caspase 8
$C8^* : CARP$	Complex of $C8^*$ and CARP
$CARP$	Caspase 8- and 10-associated RING protein
C_G^0	Concentration of glucose in environment
C_G^{ss}	Steady state concentration of glucose in a spheroid
CO^*	Activated complex of DR and T
C_T^0	Concentration of TRAIL in environment
δ	Constrictivity
D	Effective diffusion coefficient
DISC	Death-inducing signaling complex
DcR	Decoy receptor
D_G	Effective diffusion coefficient of glucose in a spheroid
DR	Death receptor

Nomenclature

$DR : T$	Complex of DR and T
D_T	Effective diffusion coefficient of TRAIL in a tumor spheroid
ε	Porosity
r	Radial variable
ECM	Extracellular matrix
FADD	Fas-associated death domain
FLIP	FLICE-like inhibitory protein
g_{max}	Maximal growth rate
g_{min}	Minimal growth rate
IAP	Inhibitor of apoptosis protein
k_{-1}	Dissociation rate
k_1	Association rate
k_2	Activation rate
k_{ext}	Maximal uptake rate of glucose
K_m	Michaelis-Menten constant for glucose uptake
k_{max}	Maximal rate for glucose uptake of one cell
k_{min}	Minimal uptake rate of glucose
k_U	Uptake rate of glucose by a single cell
MCTS	Multicellular tumor spheroid
N_A	Avogadro's number
OPG	Osteoprotegerin
PDE	Partial differential equation

R	Radius of outermost layer of simulated area
r_x	Radius of outermost layer of simulated spheroid
τ	Tortuosity
T	TRAIL molecule
t_0	Start time of simulation
$t_{division}$	Time of next division of a cell
t_{end}	End time of simulation
TNF	Tumor necrosis factor
TRAIL	TNF-related apoptois inducing ligand
UV	Ultraviolet
V	Extracellular volume per cell accesible for diffusion
x	Spatial variable
z	Number of cells in a cell layer

1 Introduction

Systems biology aims to understand biochemical processes holistically by means of mathematical models. They enable extensive analysis of complex biological systems. For example in cancer research, mathematical models can generate prognoses for the growth and behaviour of tumors under medical treatment. This can reduce the gap of therapeutic efficacy between *in vitro* experiments and real world patient treatment.

Mostly, tumor cells can be killed by inducing apoptosis. TRAIL, a potential tumor therapeutic induces apoptosis via triggering of death receptors. It is a potential therapeutic because TRAIL induces apoptosis exclusively in abnormal cells. However, cell populations in three-dimensional shapes, as multicellular tumor spheroids, show an increased resistance to medical treatment compared to two-dimensional ones. This phenomena is called multicellular resistance and occurs during treatment with drugs including TRAIL.

The profound understanding of the mechanisms in a tumor spheroid under treatment with TRAIL and their relevance for the development of the resistance could explain this phenomena. There are three characteristics of tumor spheroids which are regarded possible reasons:

1. Heterogeneous distribution of TRAIL in spheroids, especially reduced concentration in the center due to limited diffusion,
2. heterogeneity of tumor cells in the spheroid, proliferating, quiescent and necrotic cells occur due to limited nutrient supply,
3. intercellular communication, which increases anti-apoptotic signals.

A mathematical model could derive which characteristics are decisive for the development of resistance.

This work is split in two parts. The first part “Propaedeuticum” presents background information concerning cancer and mathematical modeling in cancer research in form of a review on actual and historical models considering three-dimensionality. In the second part, the Bachelor thesis “Modeling and simulation of a three-dimensional tumor spheroid” is presented. The thesis focuses on modeling and simulating the first and the second of the above mentioned

characteristics. A theoretical model is derived in Chapter 5 which represents a tumor spheroid under treatment with TRAIL. The diffusion of TRAIL and nutrients into the spheroid is modeled in Section 5.2, as well as the intracellular reaction to TRAIL stimulation and glucose uptake, see Section 5.3. The theoretical model is implemented by extending an agent-based simulation framework by Imig *et al.* (2015) by a third dimension. Following, the *in silico* model is analyzed regarding validity and computing capacity. At last, a population under treatment with TRAIL is simulated in three dimensions. The results are analyzed and compared to the two-dimensional case.

Part I

Propaedeuticum

2 Biological Background

Cancer therapy is an important and interesting research area in systems biology, in which potential drugs are analyzed via mathematical models. Since in the following chapter the modeling of tumor spheroids under medical treatment is discussed, it is essential to regard the biological processes of cancer in detail. Therefore, the first section presents development and structure of a tumor. Afterwards, the pathway of apoptosis and TRAIL (TNF-related apoptosis-inducing ligand), a potential therapeutic agent, are regarded with focus on their function in cancer therapy.

2.1 Tumor Formation

Cancer is associated with genetic alterations, which disrupt cell control mechanisms and lead to an increased proliferation rate. The affected genes are divided into two classes: proto-oncogenes and tumor suppressor genes. Usually, the protein products of proto-oncogenes stimulate cell proliferation. But proto-oncogenes can mutate into oncogenes which protein product's promote tumor growth. In addition, mutations of tumor suppressor genes, which normally signal for cell-cycle arrest or induce apoptosis, result in dysfunction of protein products causing tumor growth. For further information on deregulation of the cell cycle in cancer, Vermeulen *et al.* (2003) is recommended.

The appearance of such mutations can lead to cells with an increased proliferation rate which form an early tumor, called an avascular tumor. Since an avascular tumor only receives nutrients from surroundings by diffusion, its size is restricted to 400 – 600 μm in diameter (Nyga *et al.*, 2011). With increasing size the amount of nutrients reaching the tumor center declines. When the nutrient amount is too low to sustain the cells in the tumor center, they die and form a necrotic core. Moreover, a layer of quiescent cells separates the nutrient-starved necrotic core from a layer of proliferating cells on the outside (Sutherland *et al.*, 1986). The general structure of an avascular tumor is illustrated in Figure 2.1.

If the tumor gets vascularized, during a process of angiogenesis, in which blood vessels from adjacent vasculature grow, it gets access to nutrient source via blood circulation. The vascular tumor grows fast and can get a huge size. So

called invasive tumors, which grow into surrounding structures like vasculature, can cause metastasis (Folkman, 1974).

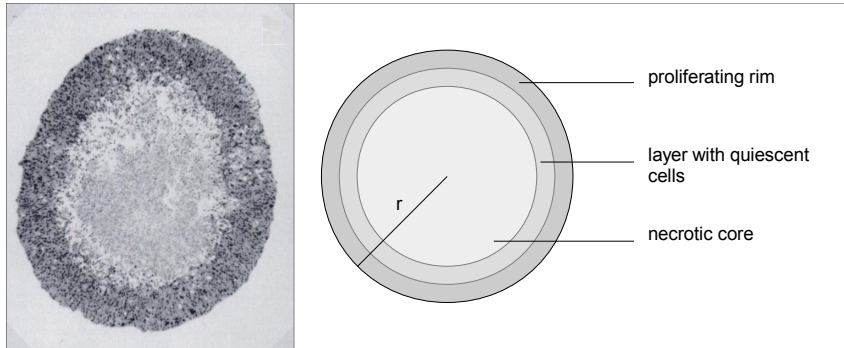


Figure 2.1: Schematic cross section of a fully-developed avascular tumor (right figure) in comparison to a central cross section of an *in vitro* spheroid (left figure). An outer rim of proliferating cells surrounds a layer of quiescent cells and a central core of necrotic cells. Left figure taken from Sutherland *et al.* (1986).

2.2 Pathway of Apoptosis

Apoptosis is a highly-regulated process of programmed cell death during which, in contrast to necrosis, no damage to the surrounding tissue occurs. It can be initiated by various intrinsic and extrinsic inducers. DNA-damage (e.g. via UV-irradiation or chemotherapy), the loss of control over cell cycle and many other internal checkpoints of cell cycle stimulate the cell-intrinsic pathway. In contrast, the cell-extrinsic pathway of apoptosis is stimulated by the triggering of death receptors (DRs) (e.g. via TRAIL or T-killer cells), the loss of survival signals by growth factors and the loss of surrounding cells (Kerr *et al.*, 1994). Figure 2.2 illustrates the cell-extrinsic and cell-intrinsic pathways of apoptosis.

Following initiation of the cell-extrinsic pathway, cytoplasmic proteins including the adaptor protein FADD (Fas-associated death domain) form a death-inducing complex (DISC) at the death domain of the receptor. Hereupon, procaspase 8 is recruited to the DISC, autoactivates by proteolysis and activates procaspase 10 by cleaving it. Activated initiator caspases 8 and 10 cleave

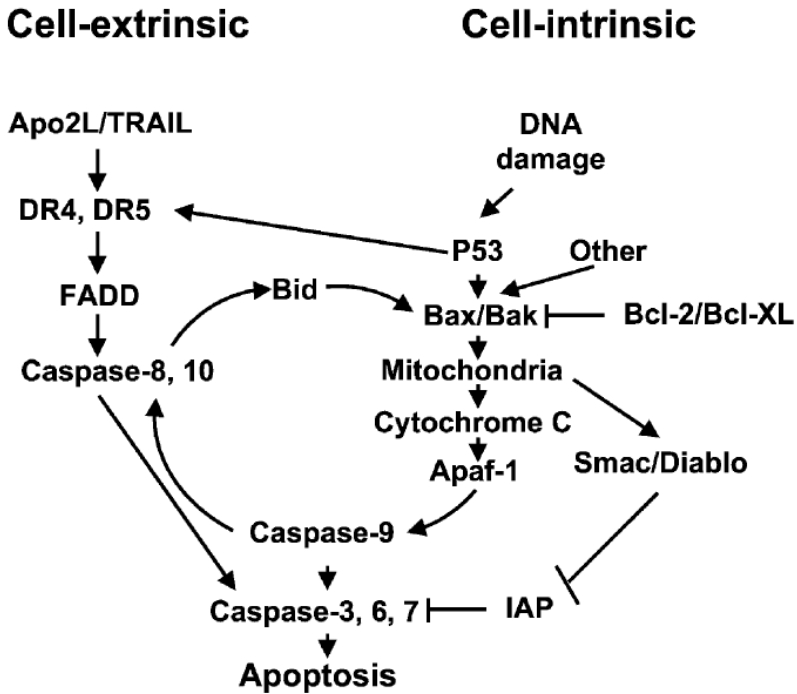


Figure 2.2: Activation of the cell-extrinsic and cell-intrinsic apoptosis pathways by Apo2L/TRAIL. Taken from Almasan & Ashkenazi (2003).

procaspases 3, 6 and 7 which work in activated form as effector caspases.

The exact procedure of apoptosis depends on the cell type. In cells of type I, activation of the extrinsic pathway is sufficient to activate the effector caspases and cause apoptosis. In contrast, in cells of type II execution of apoptosis depends on the indirectly activated intrinsic pathway and the resulting amplification of death signal.

The intrinsic pathway is on the one hand indirectly activated by initiator caspases cleaving Bid, a pro-apoptotic member of the Bcl-2 family. Cleaved Bid translocates to the mitochondria and activates Bax and Bak, pro-apoptotic members of the Bcl-2 family. On the other hand, cell-internal apoptosis initiators like DNA-damage enhance the expression of tumor suppressor gene p53 which activates Bax and Bak. Activation of Bax and Bak leads to the release of the signaling molecule cytochrome c from the mitochondrion. Bax and Bak are counteracted by anti-apoptotic members of the Bcl-2 and Bcl-XL family. The binding of cytoplasmic cytochrome c to the protein Apaf-1 initiates the formation of an apoptosome. Following, procaspase 9 is recruited to the apoptosome and activated. Caspase 9 activates procaspases 3, 6 and 7 as well as procaspases 8 and 10. The effector caspases are binded and inhibited by inhibitor of apoptosis proteins (IAPs) which in turn are inhibited by Smac/Diablo released from the mitochondrion (Almasan & Ashkenazi, 2003).

Effector caspases activated in course of cell-extrinsic or cell-intrinsic pathway, trigger the following degradation of the cell. Condensation of chromatin, DNA-laddering, cell shrinkage and formation of apoptotic bodies, finally lead to a total phagocytosis of the cell (Kerr *et al.*, 1994).

2.3 The Potential Therapeutic TRAIL

TRAIL is a potential tumor-specific cancer therapeutic because it induces cell death, more precisely apoptosis, selectively in transformed cells. The induction of apoptosis through TRAIL works by engagement of death receptors which initiates the cell-extrinsic pathway. Two of the receptors which bind TRAIL are pro-apoptotic, DR4 and DR5. The other three receptors, Decoy receptor 1 (DcR1), DcR2 and osteoprotegerin (OPG), act as “decoys” since their extracellular domains are homologous to death receptor domains but the receptors are not capable of transmitting a pro-apoptotic signal (Almasan & Ashkenazi, 2003). Figure 2.3 gives an overview of the five TRAIL receptors.

As a result of the above represented characteristics, the potential of TRAIL as cancer therapeutic is promising. While most therapeutics, as chemotherapy,

target on initiation of the intrinsic pathway, TRAIL initiates the extrinsic pathway. Further, most DNA-damaging drugs, like chemotherapy, require the function of tumor suppressor p53, whereas in most human cancers p53 is inactivated after following tumor progression or as a result of clinical treatments (Almasan & Ashkenazi, 2003). This inactivation of p53 results in a resistance to chemotherapy and as consequence all therapeutics targeting the intrinsic pathway are failing in therapy.

In conclusion, TRAIL can trigger apoptosis independent of the tumor suppressor p53 and therefore avoid the resistance. A combination of TRAIL and chemotherapy might lead to synergistic apoptosis activation and an effective tumor treatment. For further discussion on TRAIL's potential for cancer research, Almasan & Ashkenazi (2003) is recommended.

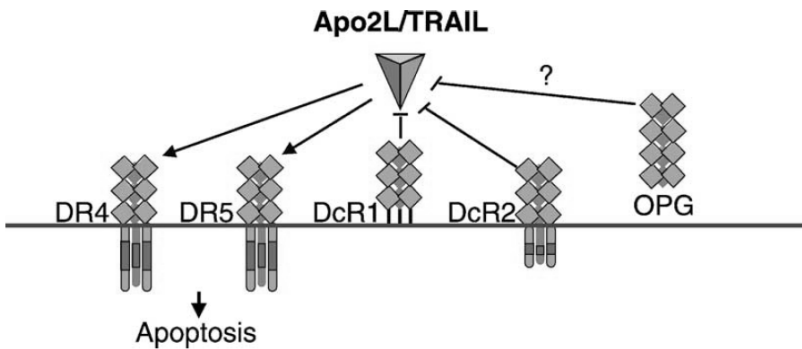


Figure 2.3: TRAIL receptors and their function. Figure taken from Almasan & Ashkenazi (2003).

3 Three-dimensional Models of Tumor Spheroids

In this chapter, models of three-dimensional tumor spheroids are presented. The first section discusses experimental *in vitro* and *in vivo* models. In the following section, *in silico* models are reviewed with focus on three-dimensional models.

3.1 Experimental Models

To calibrate and validate a mathematical model or test potential cancer therapeutics, as TRAIL, in experiments, an adequate *in vitro* model of tumors is important. Research on molecular and genetic mechanism of cancer has widely used two-dimensional models like monolayers. Monolayers are single-cell layers grown on a flat medium.

So called *in vivo* models, as human tumor xenografts, mimic the morphological characteristics and the *in situ* environment of a tumor better than two-dimensional *in vitro* models. However, since those tumors are grown in living mice, it is a challenge to observe its behaviour under medical treatment. So far, most efforts to translate results of xenograft models to the clinic failed (Nyga *et al.*, 2011).

A three-dimensional *in vitro* model is an important alternative to two-dimensional models and *in vivo* models. Multicellular tumor spheroids (MCTSs) have proved appropriate (Friedrich *et al.*, 2007). Many culture methods have been developed to generate MCTS, which are thereby easy to generate and therefore applicable in experimental research. One method aims to generate spheroids as hanging drops, wherein the cells can grow together. Their complexity ranges from MCTS consisting of a single cell line to MCTS which include multiple cell types. In addition, there are approaches to equip MCTS with proper extracellular matrix (ECM). Some are presented in Nyga *et al.* (2011). A MCTS mimics micrometastases, avascular microtumors or intercapillary tumor microregions. Further the development of rims and the appearance of concentration gradients can be observed analogously to solid tumors as imaged in

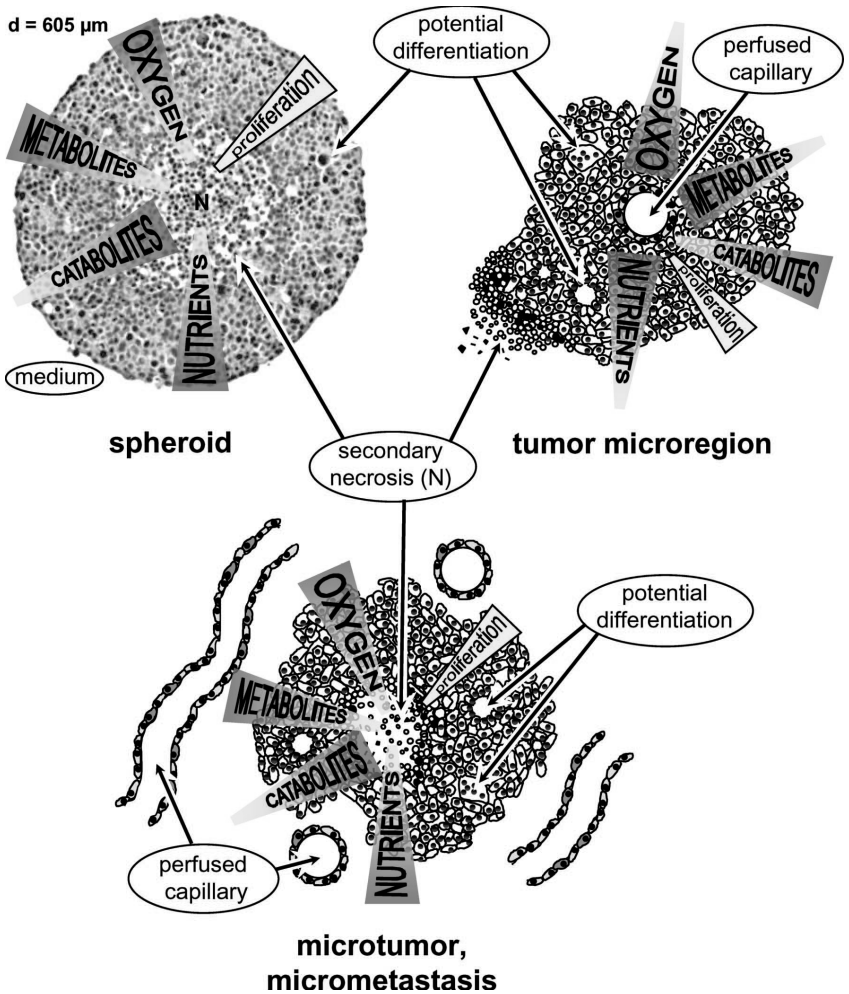


Figure 3.1: Multicellular tumor spheroids display growth characteristics and numerous pathophysiological features of avascular microtumors and developing micrometastases and also inside out resemble the situation from intercapillary tumor microregions. Taken from Friedrich *et al.* (2007).

Figure 3.1. A detailed discussion of the suitability of MCTS as *in vitro* model can be found in Friedrich *et al.* (2007).

Recent experiments with three-dimensional models showed an increased resistance to medical treatment compared to experimental results with two-dimensional models (Fessl, 2013). To understand underlying processes and the reasons for the development of this resistance, MCTSs are used for the current research.

3.2 In Silico Modeling Approaches

This section focuses on *in silico* models considering three-dimensionality of tumor spheroids. Chronologically, Shymko & Glass (1976) and Greenspan (1976) presented the first three-dimensional models of tumor spheroids (Araujo & McElwain, 2004). Both attempted to predict the growth pattern of tumor spheroids and to reveal essential mechanisms of tumor growth. Shymko & Glass (1976) extended a one-dimensional, schematic model describing the growth and development of a tumor including effects of growth inhibitors. Their three-dimensional model predicted the effect of the three-dimensional shape on stability of the spheroid during growth. Self-limiting growth in three dimensions in contrast to unlimited growth of two-dimensional populations was shown. The model of Greenspan (1976) includes various important phenomena derived in experimental work by Sutherland *et al.* (1986), such as the existence of a steady-state size, the development of a necrotic core due to limited nutrient supply and cell movement inside the spheroid. The model by Greenspan (1976) predicted stability of a spheroid to external, asymmetric perturbations. It was shown that an aggregate of cells becomes less stable with increasing size. In addition, a function of two model parameters was derived predicting whether or not a steady state size is reached before external perturbations predominate. The parameters were dependent of surface tension, external nutrient concentration, rate of volume loss due to necrosis and rates of proliferation and consumption.

Today, various *in silico* models of tumor spheroids exist focusing on the growth and development of avascular (Schaller & Meyer-Hermann, 2005; Galle *et al.*, 2005; Kim *et al.*, 2007) and vascular tumor spheroids (Shirinifard *et al.*, 2009), angiogenesis (Shirinifard *et al.*, 2009), cell migration in a spheroid (Schaller & Meyer-Hermann, 2006) or metastasis and tumor invasion (Stein *et al.*, 2007).

Different approaches for modeling tumor spheroids have been developed. They can mainly be structured by their choice of mathematical equipment into three main areas: continuum models, discrete models and hybrid models.

Whereas in continuum models partial differential equations (PDEs) are used to represent tumor spheroids, discrete models use ordinary differential equations (ODEs). The hybrid model type combines PDEs and ODEs to profit from both advantages.

Discrete models can represent the heterogeneity of individual cells as well as their interaction. Most simulation frameworks using ODEs are individual-based and implemented with a fixed spatial grid. Models using merely ODEs fail in representing a realistic shape of the spheroid and important fluid dynamics inside (Byrne *et al.*, 2006).

In contrast, continuum models are able to represent spatial dynamics as tumor cell density and concentration of nutrient distribution. By means of fluid and continuum mechanic principles, the diffusive transport of substrates in the extracellular space of the tumor spheroid can be modeled. However, continuum models cannot consider the discreteness of cells and tumor structures (Byrne, 2012). Schaller & Meyer-Hermann (2006) present a continuum model of avascular tumor spheroids assumed spherical symmetric. It describes densities of viable and necrotic cells as well as concentration of glucose and oxygen inside the spheroid. Their model is compared to an analogous, lattice-free agent-based model (ABM) regarding growth properties. For further reading on continuum models, the review of Byrne (2012) is recommended.

The hybrid model type combines ODEs and PDEs to benefit from both advantages. It is able to represent most phenomena and interactions across multiple space and time scales relevant for cancer. Rejniak & Anderson (2010) is recommended for a detailed review on hybrid models of tumor spheroids. ABMs are an example for a hybrid simulation framework. They can be structured in on-lattice ones using a fixed spatial grid and off-lattice ones disclaiming a grid. In on-lattice models, the positions of cells are fixed on the spatial grid, whereas in off-lattice ones cells are able to move free from fixed positions. For review on ABM, Zhang *et al.* (2008) is recommended. For example, Shirinifard *et al.* (2009) use a Potts model which is agent-based. It represents tumor growth and angiogenesis in three dimensions. The Potts model is an extension of the widely-used Cellular Automaton approach (CA) which uses a regular, fixed grid, e.g. a square, hexagonal or cubical grid. Each grid site in CA contains one or more cells. In contrast, in Potts model one cell ranges over multiple grid sites enabling a more detailed representation of the shape of individual cells. In addition, the model of Shirinifard *et al.* (2009) represents deformation of cells by using the concept of Effective Energies. This concept is as well widely-used in off-lattice models for representation of cell movement, deformation and interaction.

Part II

Bachelor thesis: Modeling and simulation of a three-dimensional tumor spheroid

4 Original Model

In this chapter, a short review of the original modeling framework by Imig *et al.* (2015) is presented. At first, the ODE model representing the intracellular reaction to TRAIL stimulation is described in Section 4.1. The following section reviews the simulation algorithm of the *in silico* model.

The original modeling framework represents a heterogeneous cell population, wherein intracellular protein dynamics are simulated in detail. Heterogeneity of cells is represented with focus on gene expression and cell cycle phases. The simulation reproduces a response behavior of the cell population to extrinsic, constant stimulation by TRAIL. Inheritance, cell division and cell death are considered as well. Whereas irreversible changes, as mutations within the population, direct cell-to-cell communication and morphological influences are neglected.

The modeling framework is able to realistically represent short-term and long-term response behavior of cell populations. It enables efficient analysis and simulation of population dynamics as well as state trajectories of single cells. For further reading, Imig *et al.* (2015) is recommended.

4.1 Intracellular ODE Model

As ODE model for protein signaling dynamics within a cell, the model by Eissing *et al.* (2004) is used in the original modeling framework. The model

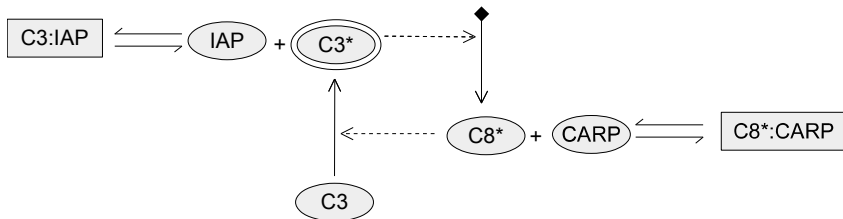


Figure 4.1: Original reaction network

reproduces the extrinsic apoptosis signaling pathway triggered by death receptor stimulation within a cell. The complex apoptotic signaling process is reduced to an elementary form, which is nevertheless able to reproduce key characteristics as bistability and a fast execution phase combined with prolonged lag phases. Consequently, this model can represent fast kinetics at the single cell level as well as slower dynamics observed in cell populations. The initial distribution of proteins are chosen heterogeneously within the population which results in individual response of cells to extrinsic stimulation.

In the following, the reaction network of the model is described. It consists of eight reactions and seven species and is illustrated in Figure 4.1. The species $C8$ represents both initiator procaspases 8 and 10. $C3$ stands in general for the executioner procaspases, e.g. 3, 6 and 7. The activated form of caspases are represented as $C3^*$ and $C8^*$. Inhibitor of apoptosis protein (IAP) represents the proteins XIAP, cIAP-1 and cIAP-2. Whereas $CARP$ is a caspase 8- and 10-associated RING protein. The species $C3 : IAP$ and $C8^* : CARP$ are complexes of the integrated proteins.

The model input is a stimulus of the receptor represented by $C8^*$ molecules. The choice of $C8^*$ molecules as model input is caused by incomplete knowledge respective the molecular events occurring around death-inducing signaling complexes (DISCs). First, $C8^*$ cleaves and activates $C3$. Further, $C3^*$ enhances the activation of $C8$. This reaction operates as positive feedback loop, whereat the effect of procaspase 6 is neglected. Moreover, the species $CARP$ and IAP both act as inhibitors by binding and cleaving $C8^*$ and $C3^*$. In this model the exceeding of a threshold of $C3^*$ represents the following apoptosis machinery, which is not simulated more detailed. The cleavage products of IAP and $C3$ are neglected. Furthermore, all species are continuously degraded, whereas $C3$, $C8$, IAP and $CARP$ are additionally synthesized. All described reactions are based on mass action kinetics.

Summarized the described reaction network of Eissing *et al.* (2004) is a very reduced system description, but nevertheless able to appropriately represent apoptosis signaling pathway. Further, the simplicity enables intense mathematical analysis within a wide range of parameters. For detailed discussion of mathematical analysis Eissing *et al.* (2004) is recommended. Hence, this ODE model is well suitable for application in the simulation.

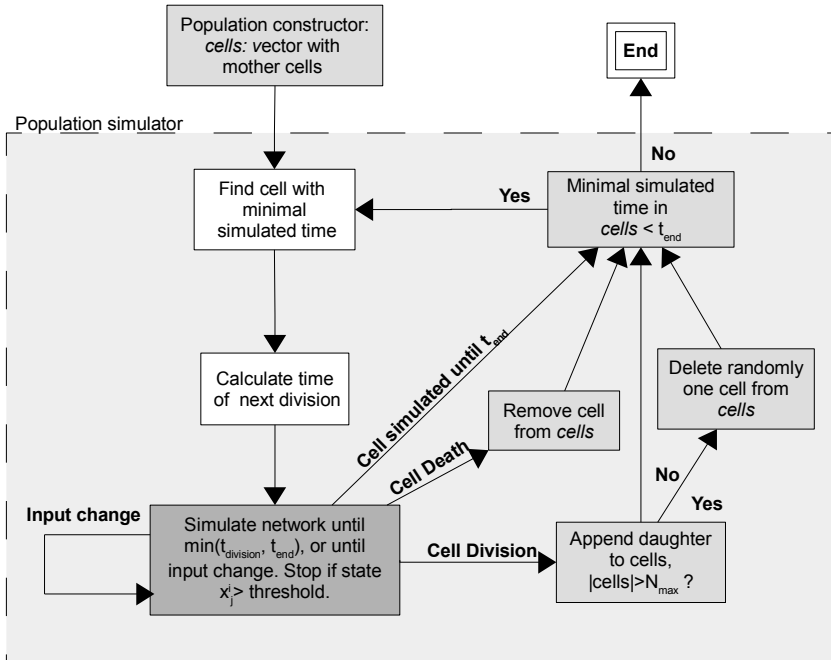


Figure 4.2: Scheme for the original simulation algorithm. Adapted from Imig *et al.* (2015)

4.2 Simulation Algorithm

This section describes the structure of the original simulation algorithm Imig *et al.* (2015) illustrated in Figure 4.2. At the beginning of the simulation, the heterogeneous cell population is constructed. Therefore, a list called *cells* is declared which contains the mother cells. In the following, the population is simulated from t_0 until t_{end} . For this purpose, the cell with minimal simulated time is chosen and its protein dynamics is calculated with the reaction network introduced in Section 4.1. It is simulated until the minimum of the time of next division $t_{division}$ and t_{end} is reached, the model input changes or the death condition is met. If a threshold of $C3^*$ is reached, the reaction network fulfills the death condition and the cell is deleted from *cells*. If otherwise the network is simulated until $t_{division}$, the cell divides. Therefore, a daughter cell is appended to *cells* and if the maximal number of cells (N_{max}) is exceeded, a random cell is removed. Hereupon, the simulation of one cell is completed for a cell cycle. In the following, all cells are simulated in the same manner until the end of population simulation t_{end} is reached. For further information on the simulation algorithm Imig *et al.* (2015) is proposed.

5 Three-dimensional Model

Experiments revealed a differing reaction of three-dimensional populations to treatment with TRAIL in contrast to the two-dimensional case, see Section 1. Three-dimensional *in vitro* models showed an emerging resistance. The main hypotheses are: reduced TRAIL concentration inside the MCTS and modified proliferation resulting from limited nutrient supply. This chapter presents the mathematical model extended with a spatial component to consider the characteristics of three-dimensional tumor spheroids leading to increased TRAIL resistance.

In the first section, MCTS as simulation object is defined. The following sections present the modeling of TRAIL and nutrient dynamics in a spheroid. The model is split into two levels. Firstly, the flow of TRAIL and glucose in the intercellular space of the tumor spheroid is simulated. This model of flow is implemented via reaction-diffusion equations presented in Section 5.2. Secondly on the cellular level, intracellular reactions following the uptake of TRAIL and nutrients into a tumor cell are considered. To implement the intracellular dynamics of TRAIL, the original reaction model 4.1 is extended and coupled to the extracellular dynamics, see Section 5.3.1. The growth rate depends linearly on the uptake of nutrients which is described in Section 5.3.2.

5.1 Biological System

As simulation object, a MCTS introduced in Section 3.1, is chosen. More precisely, an avascular tumor spheroid without a necrotic core is modeled. In experiments a necrotic core occurs when the MCTS exceeds a radius of $200\ \mu\text{m}$. Hence, the tumor spheroid is simulated up to a maximum radius of $200\ \mu\text{m}$, which correlates with 20 cell layers.

The used experimental data and hypotheses were established at the Institute of Cell Biology and Immunology of the University of Stuttgart. This specific MCTS is an appropriate choice for this work, because the institute is able to generate and test it, while it is a realistic *in vitro* model for tumor micro regions as discussed in Section 3.1. This enables a validation and verification of the results of the extended simulation model.

5.2 Model of Extracellular Substrate Dynamics

This section presents the theoretical model of TRAIL and nutrient dynamics in the extracellular space of the tumor spheroid which is developed in this thesis. The model describes the flow of the substrates TRAIL and glucose within the intercellular space of a tumor spheroid. In Section 5.2.1, the equations for the dynamics of TRAIL adapted from Goodman *et al.* (2008) are described. The system of equations consists of one partial and three ordinary differential equations. The reaction-diffusion equation derived in Section 5.2.2 is a partial differential equation and describes glucose dynamics in the intercellular space.

For simulation, the spatial dimension of the tumor population is considered. Since the detailed shape and structure of the tumor spheroid is not in focus, the spheroid is assumed to be radial symmetric. More precisely, tumor cells are regarded as spheres in a crystalline arrangement, so that the population can be portioned into cell layers. Cells with the same distance to center form a layer. The occupation of a cell layer is described as density and assumed to be homogeneous within a layer. The approximation of tumor structure is reasonable, since the detailed shape is irrelevant concerning the problem of multicellular resistance to treatment with TRAIL.

The tumor spheroid is regarded continuously porous in terms of the theory of porous media presented in Ehlers (1996). In this theory, the complex diffusion process, which takes place in the intercellular space, is replaced by a homogeneous flow through a continuum. This virtual flow is called Darcy flux. There are various approaches in the context of tumor spheroid modeling, as Goodman *et al.* (2008) and Sciumè *et al.* (2013), using the theory of porous media.

This diffusion dynamic is modeled with the second law of diffusion by Fick (1855) in one spatial dimension x :

$$\frac{\partial C}{\partial t} = \frac{\partial}{\partial x} \left[D \frac{\partial C}{\partial x} \right] \quad (5.1)$$

The diffusive transport of substrate through a tumor spheroid by Brownian motion is driven by a difference of concentration C . The substrate flows from regions with high concentration to regions with lower ones. In this equation from Grathwohl (1998),

$$D = \frac{\varepsilon \delta}{\tau} D_0 \quad (5.2)$$

is the effective diffusion coefficient which measures mobility of the diffusive substrate. In terms of the theory of porous media, the effective diffusion

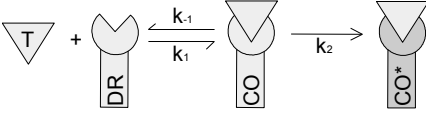


Figure 5.1: Extracellular reaction network

coefficient is a function of the porosity ε , the tortuosity τ and the constrictivity δ . Due to experimental difficulties, values of these parameters in tumor spheroids are predominantly unknown.

5.2.1 Extracellular TRAIL Dynamics

Goodman *et al.* (2008) presents a theoretical model of particle diffusion into spheroids including particle binding and association at the cell surface. In this work, the model by Goodman *et al.* (2008) is adapted to the simulation of TRAIL dynamics in the intercellular space of a tumor spheroid. In the intercellular space, the diffusion of TRAIL molecules as well as their binding to death receptors DR and the following activation of $DR : T$ -complexes (CO) is simulated. The reaction chain is visualized in Figure 5.1. The time-dependent dynamics of TRAIL

$$\begin{aligned} \frac{\partial C_T}{\partial t} &= \frac{1}{r^2} \frac{\partial}{\partial r} \left[D_T(\varepsilon) \varepsilon(\rho) r^2 \frac{\partial}{\partial r} \left[\frac{C_T}{\varepsilon} \right] \right] \\ &+ \left(k_{-1} CO - k_1 C_T \frac{N_A V}{\varepsilon} DR \right) \frac{z \varepsilon}{N_A V} \end{aligned} \quad (5.3)$$

is modeled as molar concentration C_T [$\frac{mol}{l}$]. In this equation, r is the radial direction and t is the time variable. C_T is the concentration of TRAIL molecules in the spheroid volume and $\frac{C_T}{\varepsilon}$ is the concentration of TRAIL molecules in the accessible intercellular space. z is the number of cells per cell layer, N_A is Avogadro's number and V is the extracellular space per cell. These three constants are used to transform molar concentration to molecule amount and the other way around. In this equation, non-uniformity of the spheroid is considered via the porosity ε . In Goodman *et al.* (2008), ε varies in radial direction, since different values of porosity have been determined for the proliferating and the necrotic regions. In this work, the effective porosity

$$\varepsilon(\rho) = \varepsilon_0 \rho + (1 - \rho) \quad (5.4)$$

is assumed a function of density $\rho(r)$ which also varies in radial direction r . The porosity ε_0 measures the share of a spheroids volume which makes up intercellular space in a region which is most dense (Goodman *et al.*, 2008). As it includes effects of the extracellular matrix, ε_0 cannot be calculated exactly but is determined experimentally. $\varepsilon(\rho)$ is a sum of the free space due to low cell density and the intercellular space. The effective porosity in regions with high density equals ε_0 and grows with decreasing ρ up to 1.

The effective diffusion coefficient

$$D(\varepsilon) = \varepsilon^m D_0 \tag{5.5}$$

is determined in dependence of D_0 , ε and $m \geq 0$. This equation is empirical and taken from Grathwohl (1998). It is chosen as it connects the effective diffusion coefficient directly with the porosity. The parameter m controls the porosity-dependent variation of D . For $m = 1$, the effective diffusion coefficient varies with factor 10 between most-dense regions and regions with low cell density. The effective diffusion coefficient can theoretically be measured, however in practice, experimental difficulties lead to rare knowledge of diffusion coefficients in tumor tissue.

The dynamics of death receptors DR , complexes CO and activated complexes CO^* are adapted from Aldridge *et al.* (2011) with the following ordinary differential equations using mass action kinetics:

$$\frac{\partial DR}{\partial t} = k_{-1}CO - k_1DR \cdot T + k_sDR - k_dDR \tag{5.6}$$

$$\frac{\partial CO}{\partial t} = -k_{-1}CO + k_1DR \cdot T - k_2CO - k_dCO \tag{5.7}$$

$$\frac{\partial CO^*}{\partial t} = k_2CO. \tag{5.8}$$

Figure 5.1 shows the reaction chain. The ODEs are calculated in molecule amounts per cell, so that rate values from Aldridge *et al.* (2011) can be used for the association rate k_1 , dissociation rate k_{-1} and the activation rate k_2 . The Synthesis rate k_s of DR and the degradation rates k_d of DR and CO are as well taken.

The initial and boundary conditions of C_T

$$C_T(0,r) = \begin{cases} C_T(0,1) \frac{\varepsilon(t,0)}{\varepsilon(t,0) + (\rho(1) - \rho(0)) \cdot (\varepsilon_0 - 1)} & \text{for } r = 0 \\ 0 & \text{for } r \in (0, r_x) \\ \varepsilon(0,r) \cdot C_T^0 & \text{for } r \in [r_x, R] \end{cases} \quad (5.9)$$

$$C_T(t,0) = C_T(t,1) \frac{\varepsilon(t,0)}{\varepsilon(t,0) + (\rho(1) - \rho(0)) \cdot (\varepsilon_0 - 1)} \quad (5.10)$$

$$\iff \frac{\partial}{\partial r} \left[\frac{C_T(t,0)}{\varepsilon(t,0)} \right] = 0$$

$$C_T(t,r) = \varepsilon(t,r) \cdot C_T^0 \text{ for } r \in [r_x, R]. \quad (5.11)$$

are given for the simulated area $[0, R]$ with $0 \leq r_x < R$. r_x is the radius of the outermost layer of the simulated spheroid. The simulated area is chosen major the simulated spheroid as during simulation the spheroid's size changes.

Initially, concentration of TRAIL is maximal in the surroundings of the spheroid $(r_x, R]$ and in the outermost layer with radius r_x . Inside the spheroid $[0, r_x)$, the concentration of TRAIL is initially zero.

The boundary condition for the outermost layer (5.11) is a Dirichlet condition, whereas at the most inner layer (5.10), it is a Neumann. The Neumann condition is chosen analog to Goodman *et al.* (2008).

For death receptors per cell, complexes and activated complexes the initial conditions are

$$DR(0,r) = \begin{cases} 10\,000 & r \leq r_x \\ 0 & r > r_x \end{cases} \quad (5.12)$$

$$CO(0,r) = 0 \quad \forall r \quad (5.13)$$

$$CO^*(0,r) = 0 \quad \forall r. \quad (5.14)$$

These initial conditions are given in molecule amount. The initial amount of DRs per cell is approximated by the Institute of Cell biology and Immunology.

5.2.2 Extracellular Glucose Dynamics

For simulation of nutrient supply, glucose is assumed to be the most critical nutrient for proliferation of cells in a tumor spheroid. The reason is its limited mobility in tumor tissue compared to smaller molecules like oxygen. More nutrients are theoretically easy to add, but due to missing experimental values

of diffusion coefficients in tumor tissue and uptake rates into tumor cells not implemented for now. There exist approaches modeling two or more nutrients within a spheroid, e.g. Schaller & Meyer-Hermann (2005).

Michaelis-Menten kinetics as presented in Michaelis & Menten (1913) describes the uptake rate of glucose

$$k_U(c) = c \frac{k_{max}}{K_m + c} \quad (5.15)$$

as a function of the extracellular concentration c of glucose. In this equation k_{max} is the maximum uptake rate into a cell and K_m is the Michaelis-Menten constant, which is the concentration where half of the maximum uptake rate is reached. The rate k_U as a function of c is described by a saturation curve which converges for high concentrations to k_{max} . Experimental studies, like Natarajan & Srienc (1999), prove that Michaelis-Menten kinetics adequately models the uptake of glucose into a cell.

The time-dependent dynamics of glucose concentration C_G

$$\frac{\partial C_G}{\partial t} = \frac{1}{r^2} \frac{\partial}{\partial r} \left[D_G(\varepsilon) \varepsilon(\rho) r^2 \frac{\partial}{\partial r} \left[\frac{C_G}{\varepsilon} \right] \right] - z \cdot \frac{C_G}{\varepsilon} \frac{k_{max}}{K_m + \frac{C_G}{\varepsilon}} \quad (5.16)$$

is a combination of the glucose uptake by z cells and the diffusive transport. The diffusion dynamic is modeled similar to 5.3 and taken from Goodman *et al.* (2008).

The corresponding initial and boundary conditions for glucose concentration are

$$C_G(0,r) = C_G^{ss}(r) \quad \forall r \quad (5.17)$$

$$C_G(t,0) = C_G(t,1) \frac{\varepsilon(t,0)}{\varepsilon(t,0) + (\rho(1) - \rho(0)) \cdot (\varepsilon_0 - 1)} \quad (5.18)$$

$$\iff \frac{\partial}{\partial r} \left[\frac{C_G(t,0)}{\varepsilon(t,0)} \right] = 0$$

$$C_G(t,r) = \varepsilon(t,r) \cdot C_G^0 \quad \text{for } r \in [r_x, R]. \quad (5.19)$$

The boundary conditions (5.18,5.19) are the same as for TRAIL dynamics. The steady state concentration of glucose C_G^{SS} is chosen to be the initial concentration within the spheroid. It is determined via

$$\frac{\partial C_G}{\partial t} = 0 \quad (5.20)$$

which equals the balance between glucose uptake and diffusive transport.

For simulation of the extracellular substrate dynamics, a system of two partial differential equations, 5.3 and 5.16, and three ordinary differential equations, 5.6, 5.7 and 5.8, are calculated. The dynamics of CO^* (5.8) and the uptake rate of glucose k_U (5.15) make up the interface between extracellular and intracellular model.

5.3 Model of Intracellular Substrate Dynamics

This section presents the intracellular dynamics following the uptake of TRAIL and glucose. In the original model concentrations of TRAIL and glucose are assumed homogeneous in space. This assumption results in a homogeneous growth rate and stimulation by TRAIL in population. In contrast in a three-dimensional spheroid, concentrations of TRAIL and glucose are heterogeneous and time-dependent. The intracellular reactions leading to modified cellular response to TRAIL are presented in the first part of this section. In the second part, a function is described which models the relation between the glucose uptake to a cell and its growth rate.

5.3.1 Intracellular TRAIL Dynamics

The original ODE model 4.1 is extended to enable a heterogeneous stimulation with TRAIL. For that purpose, the model input representing this stimulation is changed and the reaction network is expanded with six reactions and four species. The added reactions and species are adopted from Aldridge *et al.* (2011), a commonly used and tested model. The extended reaction network is illustrated in Figure 5.2.

In the original model, the model input is given in form of $C8^*$ molecules. Due to the nonlinear relation between TRAIL stimulation and activation of $C8$, it is not possible to stimulate the tumor cells individually within the original model. The model input is changed to activated complex molecules CO^* . Its signal strength is determined via the input rate

$$k_I = \frac{\Delta CO^*}{\Delta t} \quad (5.21)$$

which is calculated from the amount of activated molecules ΔCO^* per interval Δt . The rate k_I connects the extra- and intracellular reaction dynamics and is constant in an interval. The amount of activated molecule complexes CO^* follows from the extracellular dynamics (5.8). Intracellular reactions follow to

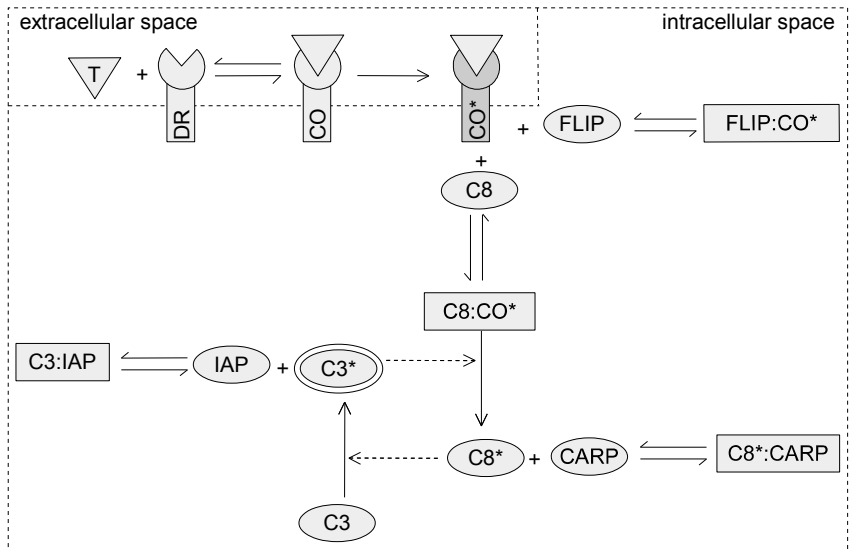


Figure 5.2: Extended reaction network. The original reaction network is extended with extracellular and intracellular reactions. The species CO^* acts in extracellular space as well as in intracellular space. All species except T are degraded, whereas $C8, C3, IAP, CARP, FLIP$ are DR continuously synthesized.

the activation of CO as illustrated in Figure 5.2. Activated complexes CO^* bind and activate $C8$. The species FLICE-like inhibitory protein (FLIP) acts as inhibitor for CO^* by binding and cleaving it. All species are continuously degraded. FLIP is continuously synthesized. Therefore, reaction, production and degradation rates are taken from Aldridge *et al.* (2011).

5.3.2 Intracellular Glucose Dynamics

Intracellular reactions following the uptake of glucose are not modeled in detail. Instead, a linear relation is deduced representing the growth rate of a cell as a function of glucose uptake. The rate of glucose uptake into one cell 5.15 is modeled with Michaelis-Menten kinetics. The growth rate of cells in relation to the extracellular substrate concentration is as well often modeled with a Michaelis-Menten kinetics. This approach of Monod (1949) is appropriate to describe growth dynamics of cell populations. In this work, the growth rate as function of the uptake rate k_U (5.15)

$$g(k_U) = \max\left(g_{min}, g_{min} + \frac{g_{max} - g_{min}}{k_{max} - k_{min}} (k_U - k_{min})\right) \quad (5.22)$$

for $k_U \in [0, k_{max}]$

is bounded above by the limitation of the uptake rate k_{max} resulting in g_{max} , the maximal growth rate. A limit below is set with regard to simulation, during which g must be positive. k_{min} is the uptake rate which is assumed for cells within the 21st layer. Cells with an uptake rate smaller than k_{min} are necrotic due to insufficient nutrient supply and not simulated in this work.

6 Implementation of Simulation Algorithm

This chapter introduces the extended simulation algorithm. In the first section, the numerical approximation of the system of differential equations derived in Section 5.2 is presented. In Section 6.2, the necessary modifications are argued, therefore the extension to a three-dimensional population and the division of simulation into intervals is discussed. The structure of the algorithm is described in Section 6.3 and illustrated in Figure 6.1.

6.1 Numerical Solution

In this section, the numerical solution of extracellular substrate dynamics, as described in Section 5.2, is presented.

At first, the simulated area is discretized in spatial dimension. Therefore, it is split in cell layers with discrete radius r and constant thickness Δr in terms of the finite difference method. Within one cell layer the concentration of glucose and TRAIL is assumed constant. For further information on the finite difference method, Schwarz & Köckler (2011) is recommended.

As merely the diffusive terms of the reaction-diffusion equations for TRAIL and glucose (5.3) and (5.16) include spatial derivatives, the finite difference approximation is restricted to these terms. To enable application of the finite difference method, the diffusive term is transformed:

$$\begin{aligned}
 & \frac{1}{r^2} \frac{\partial}{\partial r} \left[D(\varepsilon) \varepsilon(\rho) r^2 \frac{\partial}{\partial r} \left[\frac{C}{\varepsilon} \right] \right] & (6.1) \\
 &= \frac{\partial D}{\partial r} \varepsilon \frac{\partial}{\partial r} \left[\frac{C}{\varepsilon} \right] + D \frac{\partial \varepsilon}{\partial r} \frac{\partial}{\partial r} \left[\frac{C}{\varepsilon} \right] + \frac{2}{r} D \varepsilon \frac{\partial}{\partial r} \left[\frac{C}{\varepsilon} \right] + D \varepsilon \frac{\partial^2}{\partial r^2} \left[\frac{C}{\varepsilon} \right] \\
 &= m D_0 (\varepsilon_0 - 1) \frac{\partial \rho}{\partial r} \varepsilon^m \frac{\partial}{\partial r} \left[\frac{C}{\varepsilon} \right] + D (\varepsilon_0 - 1) \frac{\partial \rho}{\partial r} \frac{\partial}{\partial r} \left[\frac{C}{\varepsilon} \right] + \frac{2}{r} D \varepsilon \frac{\partial}{\partial r} \left[\frac{C}{\varepsilon} \right] \\
 &+ D \left(\frac{\partial^2 C}{\partial r^2} - \frac{2}{\varepsilon} (\varepsilon_0 - 1) \frac{\partial \rho}{\partial r} \frac{\partial C}{\partial r} - \frac{C}{\varepsilon} (\varepsilon_0 - 1) \frac{\partial^2 \rho}{\partial r^2} + \frac{2C}{\varepsilon} (\varepsilon_0 - 1)^2 \left(\frac{\partial \rho}{\partial r} \right)^2 \right)
 \end{aligned}$$

$$\text{with } \frac{\partial}{\partial r} \left[\frac{C}{\varepsilon} \right] = \frac{1}{\varepsilon^2} \left(\frac{\partial C}{\partial r} \varepsilon - (1 - \varepsilon_0) \frac{\partial \rho}{\partial r} C \right) \quad (6.2)$$

In the following, the first spatial derivatives $\frac{\partial \rho}{\partial r}$ and $\frac{\partial C}{\partial r}$ are replaced by the first-order central difference (Schwarz & Köckler, 2011):

$$\frac{\partial x}{\partial r} \approx \frac{x(r+1) - x(r-1)}{2\Delta r} \quad (6.3)$$

In addition, the second spatial derivatives $\frac{\partial^2 \rho}{\partial r^2}$ and $\frac{\partial^2 C}{\partial r^2}$ are replaced by the second-order difference (Schwarz & Köckler, 2011):

$$\frac{\partial^2 x}{\partial r^2} \approx \frac{x(r-1) - 2x(r) + x(r+1)}{(\Delta r)^2} \quad (6.4)$$

For solving the set of discretized equations at discrete time points t two different methods are implemented. On the one hand, the explicit Euler method is implemented. For this method regular time intervals Δt are chosen, wherein ΔC , ΔDR , ΔCO , ΔCO^* are computed. The value X at time point $t+1$

$$X^{t+1} = X^t + \Delta X \quad (6.5)$$

is determined from the value at time point t . Further informations on the explicit Euler method are given in Zulehner (2011).

On the other hand, a method based on backwards differentiation formulas (BDF) with adaptive step size is implemented. For further information on this method, the SUNDIALS library (<http://sundials.wikidot.com/bdf-method>) is recommended.

6.2 Modifications

For simulation of the three-dimensional model, the algorithm is modified and extended. First, the population is extended to a spatial dimension. The original population is portioned into cell layers and the population is extended with the variables *density* and *radius*. The variable *radius* assigns each cell a layer and the variable *density* stores the occupation of cell layers. Since the space within a layer is limited, proliferation can lead to sliding of tumor cells within the spheroid. The daughter cell arises in the layer of its mother cell and if this layer is fully occupied, a random cell from the layer is relocated to a neighboring layer. This is proceeded within each affected layer until a subtotal occupied layer is reached. Whether the cells are moved inwards or outwards is randomly decided with a probability of 70:30 (inwards:outwards). This procedure guarantees, that resistant genetic mutations occurring in one cell layer not unnaturally spread to distant layers.

Further, the simulation of extracellular TRAIL and glucose dynamics is added. The presented system of differential equations from Section 5.2 are calculated as presented in Section 6.1 to simulate the flow of TRAIL and glucose within a tumor spheroid. This simulation results in a heterogeneous distribution of TRAIL and glucose in the spheroid. The modified extracellular TRAIL and glucose dynamics are dependent on density. As a result, death and division of a cell directly influences the extracellular flow of substrate. This increased or decreased flow affects the other cells in this layer.

These variations demand the simulation of population to pass of in the real temporal order. In the original simulation the temporal order of the events are not considered, as events do not influence other cells. Since the temporal order of events is not predictable prior simulating intracellular dynamics of all cells, an approximation is implemented. The simulation of population is split into intervals. Each interval represents a time period within events pass in random order and the number of events is restricted. This guarantees an approximately real temporal order of events over the whole simulation. The order of events converges to the real order, when scaling down the length of one interval. Per interval and cell layer, constant values for the growth rate \bar{g} and the rate of model input \bar{k}_I are used, since constant values are required for the original population simulator. Mean values

$$\bar{x} = \frac{\sum_i x_i}{n} \quad (6.6)$$

are calculated using x_i , the value at every time step Δt and n , the amount of time steps.

6.3 Structure

In this section, the structure of the simulation algorithm is described and illustrated in Figure 6.1. In the beginning of the simulation a three-dimensional population is constructed. Next, the time for population simulation is split into regular intervals.

The simulation of one interval begins with the calculation of the extracellular dynamics of TRAIL and glucose assuming a constant *density*. As the population simulator needs constant values, mean values for the rate of model input and growth rate for each cell layer are determined.

Next, the population is simulated for the current interval with the constant rate of model input and the constant growth rate per cell layer. Thereby the

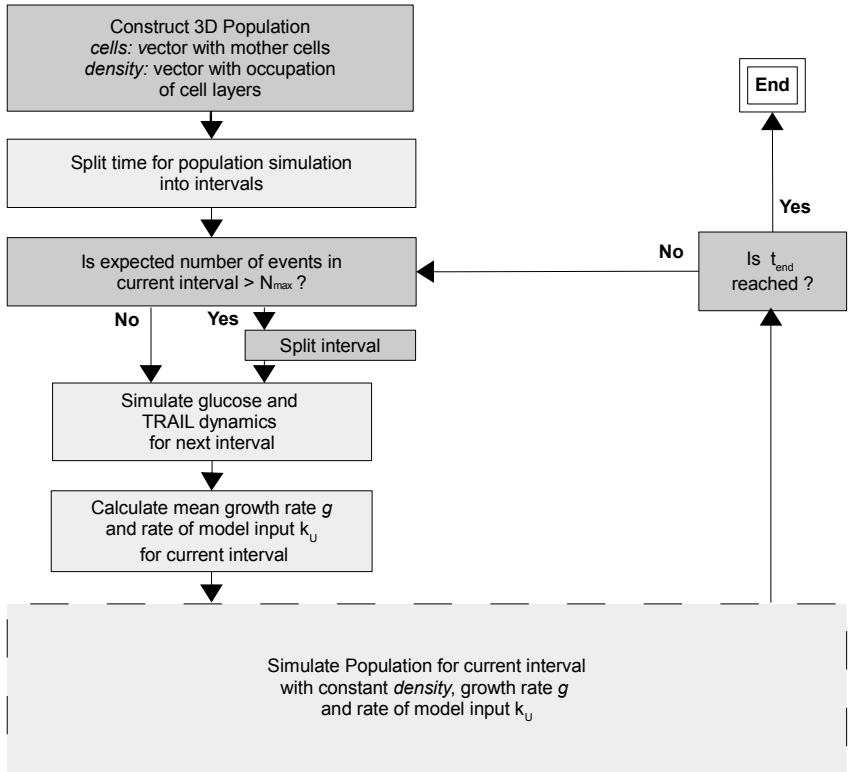


Figure 6.1: Scheme for the extended simulation algorithm

simulation proceeds like the original population simulation described in Section 4.2. Merely the variable *density* is updated past division or death. In the event of division within a completely occupied layer, cells are slid one layer. If all cells are simulated, the end of a interval is reached.

If the number of events in the last interval exceeded a treshold, the next interval is split into regular parts. The following intervals are simulated in the same manner until the end of the simulation t_{end} is reached.

7 Parameter and Validation

This chapter presents the parameters used for simulation and resulting simulations which are proper for validation. In most cases, experimentally determined parameters are taken from various research papers. However, some of those experimentally determined values cause unrealistic simulation results. For example, measured values for the diffusion coefficients resulted in physically unrealistic high concentrations inside the spheroid in the simulation. On the one hand, this could be caused from imprecise measuring and differing experimental conditions. On the other hand, approximations assumed in the course of mathematical modeling and numerical solution could cause those incorrect results. These undefined parameters are varied and the simulation result is fitted to experimental measurements. In the following sections, the resulting parameter values and the related validation results are presented. Section 7.1 presents the parameter set for the dynamics of glucose and 7.2 presents the parameter set for TRAIL dynamics.

7.1 Concentration of Glucose, Uptake Rate and Growth Rate

The set of parameters for glucose dynamics is summarized in Table 7.1. C_G^0 is the concentration of glucose in the spheroid's environment. Its value is chosen equivalent to experimental conditions at the Institute of Cell Biology and Immunology. The parameters describing the tumor spheroid, the porosity ε_0 and the thickness of a cell layer Δx are the same for simulation of TRAIL and glucose dynamics. The value for the porosity of the spheroid ε_0 is taken from Goodman *et al.* (2008). The Michaelis Menten constant for glucose uptake K_m is taken from Li (1982).

The values for D_G and k_{max} are adapted, since the experimentally determined values of Casciari (1988) and Li (1982) result in a steady state distribution without reduction of concentration inside the spheroid. Therefore, a most dense spheroid with 20 cell layers is simulated. With the fitted values of D_G and k_{max} , a steady state distribution illustrated in Figure 7.1 is reached after about 2,5 *min*. The value in the center of the spheroid is $\sim \frac{1}{6}C_G^0$ which is similar to distributions found in Li (1982).

Parameter	Symbol	Value
Concentration of glucose in environment	C_G^0	11,1111 mM
Effective diffusion coefficient of glucose in a tumor spheroid	D_G	$2,3E - 10 \frac{m^2}{s}$
Maximal rate for glucose uptake of one cell	k_{max}	$3E - 8 \frac{mol}{cell*s}$
Michaelis-Menten constant for glucose uptake	K_m	0,58 mM
Maximal uptake rate of glucose	k_{ext}	$2,8512E - 08 \frac{mol}{cell*s}$
Minimal uptake rate of glucose	k_{min}	$2,27612E - 08 \frac{mol}{cell*s}$
Maximal growth rate	g_{max}	$6,5359E - 4 \frac{1}{min}$
Minimal growth rate	g_{min}	$2,8881E - 4 \frac{1}{min}$
Porosity of tumor spheroid	ε_0	0,1
Thickness of a cell layer	Δx	$1E - 5 m$

Table 7.1: Parameter set for glucose dynamic

The distribution of glucose uptake per cell illustrated in Figure 7.2 is calculated from the steady state concentration C_G^{SS} . k_{ext} is the uptake rate in the outermost layer and k_{min} is the critical uptake rate per cell which shows up in the 21st layer. The growth rate is linearly linked to the rate of glucose uptake. The maximal growth rate g_{max} equals the growth rate of a cell in a two-dimensional, monolayer population. It corresponds with 17,6754 h per cell cycle. The minimal growth rate g_{min} is equivalent to 40 h per cell cycle.

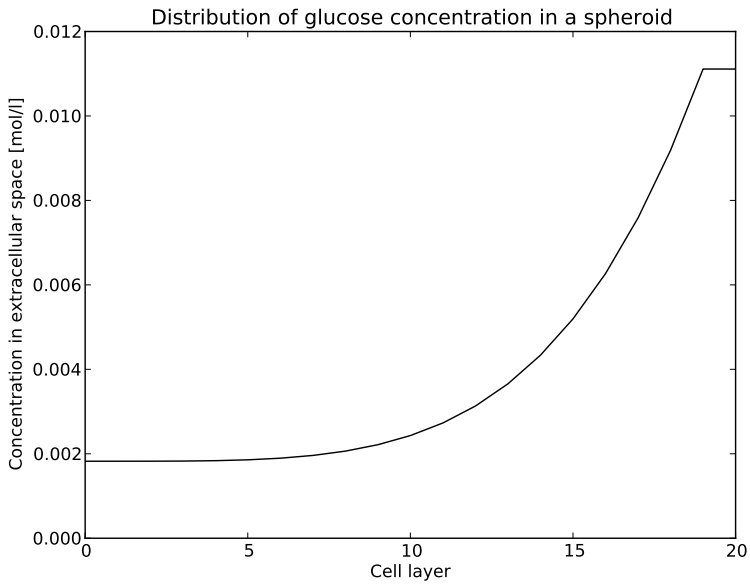


Figure 7.1: Steady state distribution of glucose concentration in a spheroid with 20 cell layers

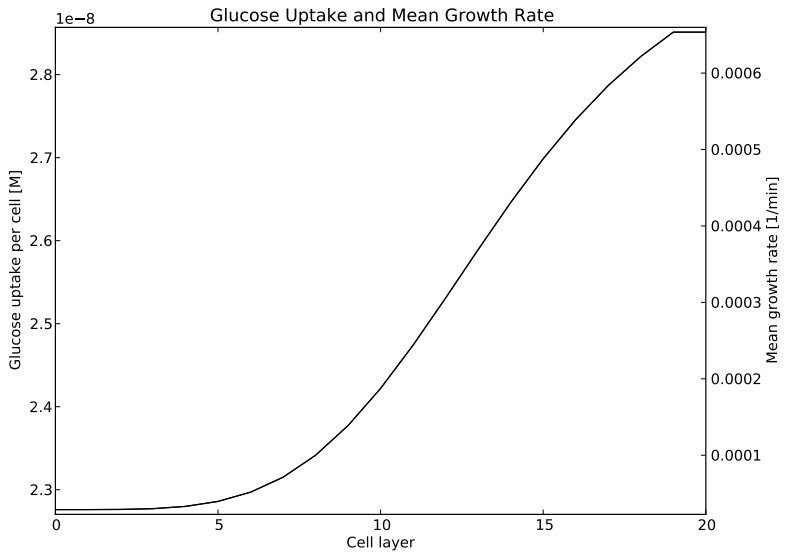


Figure 7.2: Steady state rates of glucose uptake and cell growth in a spheroid with 20 cell layers.

7.2 TRAIL Concentration

Parameter	Symbol	Value
Effective diffusion coefficient of TRAIL in a tumor spheroid	D_T	$3E - 14 \frac{m^2}{s}$
Concentration of TRAIL in environment	C_T^0	$0,2 nM$
Extracellular volume per cell accesible for diffusion	V	$4E - 18 \frac{m^3}{l}$
Association rate	k_1	$4E - 7 \frac{molec}{s \cdot cell}$
Dissociation rate	k_{-1}	$0,001 \frac{1}{s}$
Activation rate	k_2	$5E - 5 \frac{1}{s}$
Porosity of tumor spheroid	ε_0	$0,1$
Thickness of a cell layer	Δx	$1E - 5 m$

Table 7.2: Parameter set for TRAIL dynamics

Table 7.2 shows the parameter set used for simulation of TRAIL dynamics. The concentration of TRAIL in environment C_T^0 is chosen equivalent to experimental conditions. Association rate k_1 , dissociation rate k_{-1} and activation rate k_2 are taken from Aldridge *et al.* (2011).

The diffusion coefficient D_T is adapted since the experimental determined diffusion coefficient of Albumin in tumor spheroids of Davies *et al.* (2002) resulted in obviously to fast diffusive transport in simulation. A spheroid with 20 fully occupied cell layers is simulated for 24h and 96h. Thereby, only the diffusion without the reaction is simulated, so that the concentration inside the spheroid can be fitted to experiments of Albumin diffusion into tumor spheroids as seen in Fessler (2013). Figure 7.3 presents the resulting TRAIL concentrations after 24h and 96h.

V , the extracellular space per cell could be theoretically calculated from the volume of a spheroid and the effective porosity, but due to imprecise values, it is adapted. As V influences the transformation of molar concentration into molecule amounts, its exact determination is important. Therefore a two-dimensional population is extended with the dynamics of DR , CO and CO^* and its behaviour under treatment with TRAIL is fitted to experiments with monolayers under TRAIL treatment. The used experimental data was established by Fabian Richter for the Institute of Cell Biology and Immunology

and has not been published yet. Figure 7.4 shows the result of fitting.

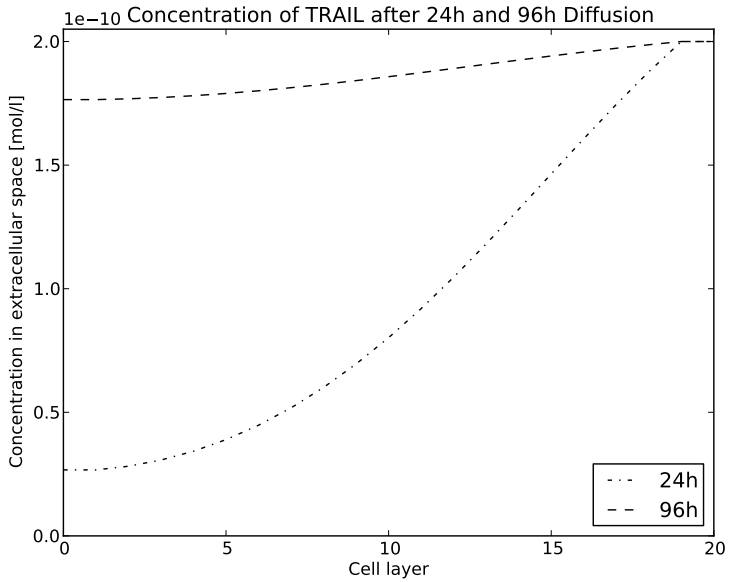


Figure 7.3: Concentration of TRAIL after 24h and 96h diffusion

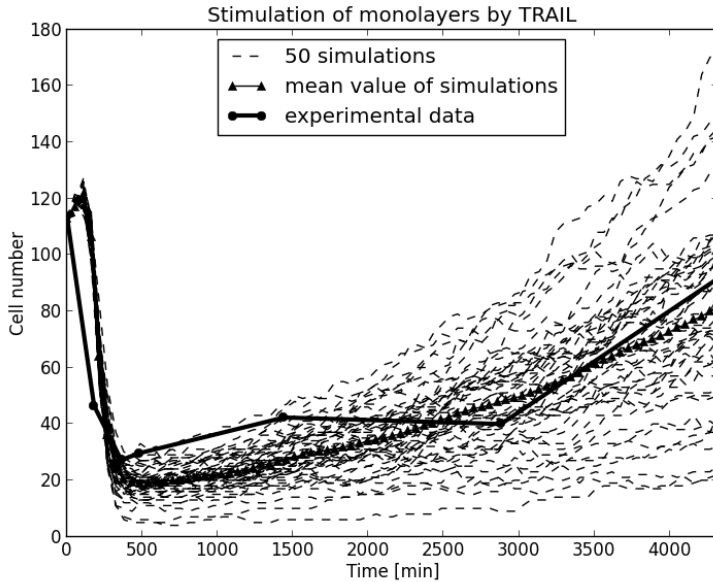


Figure 7.4: Monolayer under TRAIL treatment with extended intracellular ODE model. The used experimental data (unpublished) shows one exemplary measurement of the cell line HCT-116 and was established by Fabian Richter for the Institute of Cell Biology and Immunology.

8 Analysis and Simulation

In this chapter, the simulation is analyzed and simulation results are presented. In the first section, the computational effort of a three-dimensional simulation is analyzed and compared to the two-dimensional one. At first, the computational effort due to simulation of nutrient and TRAIL dynamics is described. In the next step, the computational effort due to changes in the simulation algorithm, mainly the division of simulation into intervals is analyzed. Section 8.2 presents simulation results comparing the reaction of a 2D population and a 3D population to TRAIL stimulation.

8.1 Analysis of Computational Effort

The computing effort due to simulation of nutrient and TRAIL dynamics is analyzed at first. Therefore, diffusion-reaction dynamics of TRAIL and glucose in a spheroid of 20000 cells are simulated for $1h$. Each dynamic is simulated with the two numerical methods described in Section 6.1. All simulations are executed on a computer with 12 Cores and 32 GB RAM. The required computing times are presented in Table 8.1.

	TRAIL dynamic	Glucose dynamic
explicit method	133,1376 s	9,5992 s
bdf method	60,3578 s	34,6742 s

Table 8.1: Computing time of reaction-diffusion dynamics

The explicit method produces different computing times of TRAIL and glucose dynamics caused by the different choice of temporal step sizes Δt . For simulation of glucose diffusion, a fixed step size of $\Delta t = 6e - 2 s$ is used, whereas TRAIL dynamic is simulated with a step size of $\Delta t = 6e - 3 s$. The fixed step size is chosen with regard to the convergence of solution. This convergence is dependent on the diffusion coefficient and the spatial step size, as well as on the simulation period and the growth dynamics of population.

The bdf method uses adaptive step sizes. This results in reduced computing times of TRAIL dynamics compared to the explicit method. The computational effort of glucose dynamics with the bdf method is increased compared to the explicit method. In addition, the distribution of concentration is approximated more exactly than the one with the explicit method. A probable reason for the different effect of the bdf method on TRAIL and glucose dynamics, is that TRAIL dynamic requires step sizes within a greater range. Further, the computing times of glucose dynamics with bdf method are higher than TRAIL dynamics. This is caused by faster dynamics of glucose diffusion compared to TRAIL diffusion.

In the following, the change of computational effort due to changes in the simulation algorithm are analyzed. Therefore, a three-dimensional simulation is executed in various amounts of intervals. A population of 20000 cells is simulated for 24 h with stimulation by TRAIL. The required computing times are given in Table 8.2.

Number of intervals	Computing time
1	128,2633 min
2	136,0378 min
10	143,6203 min
100	279,4758 min
1000	1528,9925 min

Table 8.2: Computing time of intervals

The split of simulation into intervals increases the computational effort. The increase is clearly observable from 100 intervals rising.

8.2 Simulation

In this section, the result of one exemplary simulation is presented. A population of 5000 cells is simulated for 72 h under TRAIL treatment. It is simulated in two dimensions as well as in three dimensions. The results are illustrated in Figure 8.1.

At the end of the three-dimensional simulation, about 39700 cells are alive, whereas 12400 cells have died during treatment with TRAIL. The three-dimensional simulation compared to the two-dimensional one shows an increased resistance to treatment with TRAIL. The resulting concentration of TRAIL

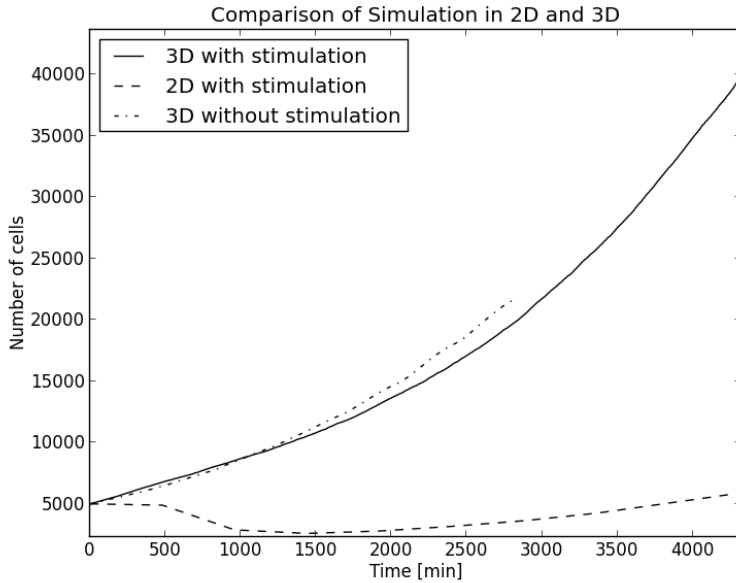


Figure 8.1: Comparison of Simulation in 2D and 3D. A cell population is simulated for 72 h in two dimensions and three dimensions with stimulation by TRAIL. In addition, the three-dimensional population is simulated for 48 h without stimulation .

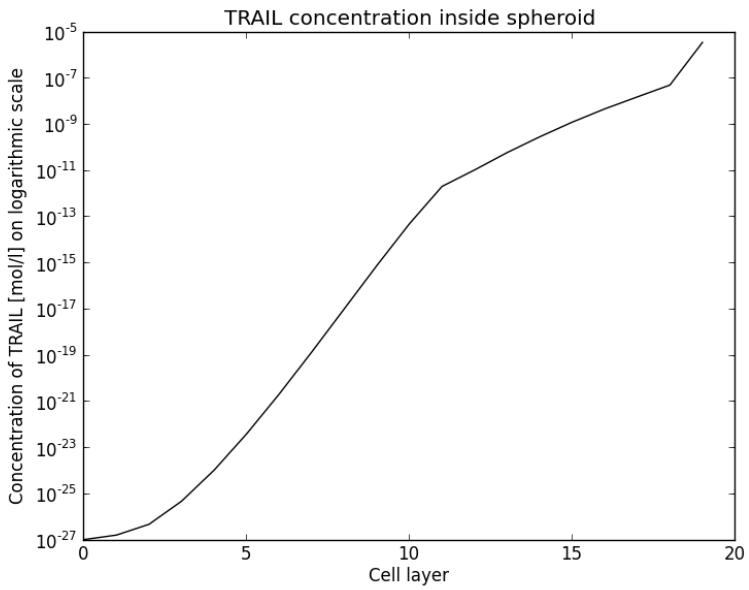


Figure 8.2: TRAIL concentration in the spheroid after 72h simulation

inside the spheroid after 72 *h* simulation in three dimensions is shown in Figure 8.2. The extremely low concentration inside the spheroid explains the similarity between the three-dimensional simulations with and without stimulation by TRAIL. The simulation results in comparison to experimental data let assume that not all simulation parameter are chosen correctly. Experimental work by Daniela Stöhr (Institute of Cell Biology and Immunology) showed an reduction of three-dimensional populations of about 40 – 75 % after 24 *h* stimulation by 0.1 *nM* TRAIL (unpublished data). This reduction of cell amount cannot be observed in simulation. One hypotheses is that the real diffusion dynamic of TRAIL is faster than assumed in simulation. Important parameters which should be adapted are the diffusion coefficient of TRAIL D_T and the minimal growth rate g_{min} .

9 Summary, Conclusions and Outlook

In this thesis, a three-dimensional mathematical model of substrate diffusion into a spheroid is derived as well as an extension of an agent-based simulation framework. The mathematical model representing the diffusion of TRAIL and glucose into a multicellular spheroid is based on reaction-diffusion equations. The spheroid is assumed radially symmetric and continuously porous in terms of the theory of porous media. The model accounts for radially dependent changes of cell density inside the spheroid which occur during simulation of the population under medical treatment. The hybrid, agent-based simulation represents a simplified, three-dimensional population under treatment with TRAIL. Therefore, the intracellular reaction to TRAIL and glucose uptake is simulated as well as TRAIL and glucose dynamics in the intracellular space. For numerical solution of the mathematical model during simulation different methods are implemented. The derived model is elementary adapted to experimental data of diffusion into spheroids. However, for a realistic adaption, more experimental data is necessary. The definite determination of all parameters is not part of this thesis.

In conclusion, the adapted model can be used to analyze the effect of TRAIL and glucose dynamics to multicellular resistance. In addition, the characteristics of 3D populations after stimulation by TRAIL can be analyzed.

In further research, the model could be adapted to equivalent experimental data. The realistic representation of TRAIL concentration in the spheroid is considered most important. Therefore, more experimental research about TRAIL diffusion in various areas of a spheroid is necessary. In addition, it could be necessary to extend the model with extracellular matrix components to realistically represent TRAIL dynamics in the spheroid.

Further, the model could be extended with intercellular communication increasing pro-apoptotic signals in the spheroid. This could be another possible reason for the increased resistance of three-dimensional populations to TRAIL stimulation. In course of this extension, the parallel implementation of contact inhibition of growth as seen in Schaller & Meyer-Hermann (2006) is proposed. This could as well result in a more realistic growth behaviour of the spheroid.

In the next step, the computing capacity of the simulation could be improved.

Therefore, the choice of the numerical method should be reviewed.

Bibliography

- Aldridge, B. B., Gaudet, S., Lauffenburger, D. A., & Sorger, P. K. 2011. Lyapunov exponents and phase diagrams reveal multi-factorial control over TRAIL-induced apoptosis. *Molecular Systems Biology*, **7**(1).
- Almasan, Alexandru, & Ashkenazi, Avi. 2003. Apo2L/TRAIL: apoptosis signaling, biology, and potential for cancer therapy. *Cytokine & growth factor reviews*, **14**(3), 337–348.
- Araujo, RP, & McElwain, DLS. 2004. A history of the study of solid tumour growth: the contribution of mathematical modelling. *Bulletin of mathematical biology*, **66**(5), 1039–1091.
- Byrne, Helen M. 2012. Mathematical biomedicine and modeling avascular tumor growth.
- Byrne, H.M, Alarcon, T, Owen, M.R, Webb, S.D, & Maini, P.K. 2006. Modelling aspects of cancer dynamics: a review. *Philosophical Transactions of the Royal Society A: Mathematical, Physical and Engineering Sciences*, **364**(1843).
- Casciari. 1988. Glucose Diffusivity in Multicellular Tumor Spheroids. *Cancer Research*.
- Davies, C de L, Berk, D A, Pluen, A, & Jain, R K. 2002. Comparison of IgG diffusion and extracellular matrix composition in rhabdomyosarcomas grown in mice versus in vitro as spheroids reveals the role of host stromal cells. *Br J Cancer*, **86**(10), 1639–1644.
- Ehlers. 1996. Grundlegende Konzepte in der Theorie Poröser Medien.
- Eissing, Thomas, Conzelmann, Holger, Gilles, Ernst D., Allgöwer, Frank, Bullinger, Eric, & Scheurich, Peter. 2004. Bistability Analyses of a Caspase Activation Model for Receptor-induced Apoptosis. *Journal of Biological Chemistry*, **279**(35), 36892–36897.

- Fessler, Sanja. 2013. *Investigation of multicellular resistance to and scFvEGFR-scTRAIL using multicellular*. M.Phil. thesis.
- Fick, Adolf. 1855. Ueber Diffusion. *Annalen der Physik*, **170**(1), 59–86.
- Folkman, Judah. 1974. Tumor Angiogenesis. *Advances in Cancer Research*, vol. 19. Academic Press.
- Friedrich, Juergen, Ebner, Reinhard, & Kunz-Schughart, Leoni A. 2007. Experimental anti-tumor therapy in 3-D: spheroids-old hat or new challenge? *International journal of radiation biology*, **83**(11-12), 849–871.
- Galle, Jörg, Loeffler, Markus, & Drasdo, Dirk. 2005. Modeling the Effect of Deregulated Proliferation and Apoptosis on the Growth Dynamics of Epithelial Cell Populations In Vitro. *Biophysical Journal*, **88**(1).
- Goodman, Thomas T., Chen, Jingyang, Matveev, Konstantin, & Pun, Suzie H. 2008. Spatio-temporal modeling of nanoparticle delivery to multicellular tumor spheroids. *Biotechnol. Bioeng.*, **101**(2).
- Grathwohl, Peter. 1998. *Diffusion in natural porous media: contaminant transport, sorption/desorption and dissolution kinetics*. Boston [u.a.]: Kluwer.
- Greenspan, H.P. 1976. On the growth and stability of cell cultures and solid tumors. *Journal of Theoretical Biology*, **56**(1), 229 – 242.
- Imig, D., Pollak, N., Strecker, T., Scheurich, P., Allgöwer, F., & Waldherr, S. accepted for publication in 2015. Individual-based simulation framework for dynamic and heterogeneous cell populations during and extrinsic stimulations. *Journal of Coupled Systems and Multiscale Dynamics*. accepted for publication.
- Kerr, John F. R., Winterford, Clay M., & Harmon, Brian V. 1994. Apoptosis. Its significance in cancer and cancer Therapy. *Cancer*, **73**(8), 2013–2026.
- Kim, Y., Stolarska, M. A., & Ohmer, H. G. 2007. A hybrid model for tumor spheroid growth in vitro I: Theoretic development and early results. *Mathematical Models and Methods in Applied Sciences*, **17**(supp01), 1773–1798.
- Li, Conan K. N. 1982. The glucose distribution in 9l rat brain multicell tumor spheroids and its effect on cell necrosis. *Cancer*, **50**(10), 2066–2073.

- Michaelis, Leonor, & Menten, Maud L. 1913. Die kinetik der invertinwirkung. *Biochem. z.*, **49**(333-369), 352.
- Monod, Jacques. 1949. The growth of bacterial cultures. *Annual Reviews in Microbiology*, **3**(1), 371–394.
- Natarajan, Arvind, & Srienc, Friedrich. 1999. Dynamics of Glucose Uptake by Single *Escherichia coli* Cells. *Metabolic engineering*, **1**(4), 320–333.
- Nyga, Agata, Cheema, Umer, & Loizidou, Marilena. 2011. 3D tumour models: novel in vitro approaches to cancer studies. *J. Cell Commun. Signal.*, **5**(3).
- Rejniak, Katarzyna A., & Anderson, Alexander R. A. 2010. Hybrid models of tumor growth. *WIREs Syst Biol Med*, **3**(1).
- Schaller, G., & Meyer-Hermann, M. 2006. Continuum versus discrete model: a comparison for multicellular tumour spheroids. *Philosophical Transactions of the Royal Society A: Mathematical, Physical and Engineering Sciences*, **364**(1843).
- Schaller, Gernot, & Meyer-Hermann, Michael. 2005. Multicellular tumor spheroid in an off-lattice Voronoi-Delaunay cell model. *Phys. Rev. E*, **71**(5).
- Schwarz, Hans Rudolf, & Köckler, Norbert. 2011. *Numerische Mathematik*. 8., aktualisierte aufl. edn. Wiesbaden: Vieweg + Teubner.
- Sciumè, G, Shelton, S, Gray, W G, Miller, C T, Hussain, F, Ferrari, M, Decuzzi, P, & Schrefler, B A. 2013. A multiphase model for three-dimensional tumor growth. *New Journal of Physics*, **15**(1), 015005.
- Shirinifard, Abbas, Gens, J. Scott, Zaitlen, Benjamin L., PopÅawski, Nikodem J., Swat, Maciej, & Glazier, James A. 2009. 3D Multi-Cell Simulation of Tumor Growth and Angiogenesis. *PLoS ONE*, **4**(10).
- Shymko, R.M., & Glass, Leon. 1976. Cellular and geometric control of tissue growth and mitotic instability. *Journal of Theoretical Biology*, **63**(2), 355 – 374.
- Stein, Andrew M., Demuth, Tim, Mobley, David, Berens, Michael, & Sander, Leonard M. 2007. A Mathematical Model of Glioblastoma Tumor Spheroid Invasion in a Three-Dimensional In Vitro Experiment. *Biophysical Journal*, **92**(1).

- Sutherland, R. M., Sordat, B., Bamat, J., Gabbert, H., Bourrat, B., & Mueller-Klieser, W. 1986. Oxygenation and Differentiation in Multicellular Spheroids of Human Colon Carcinoma. *Cancer Research*, **46**(10), 5320–5329.
- Vermeulen, Katrien, Van Bockstaele, Dirk R., & Berneman, Zwi N. 2003. The cell cycle: a review of regulation, deregulation and therapeutic targets in cancer. *Cell proliferation*, **36**(3), 131–149.
- Zhang, Le, Wang, Zhihui, Sagotsky, Jonathan A., & Deisboeck, Thomas S. 2008. Multiscale agent-based cancer modeling. *J. Math. Biol.*, **58**(4-5).
- Zulehner, Walter. 2011. *Numerische Mathematik: Eine Einführung anhand von Differentialgleichungsproblemen Band 2: Instationäre Probleme*. Basel: Springer Basel.